Harmonic wavelet analysis of modulated tunable diode laser absorption spectroscopy signals

Hong Duan, Anish Gautam, Benjamin D. Shaw,* and Harry H. Cheng

University of California, Davis, California 95616, USA

*Corresponding author: bdshaw@ucdavis.edu

Received 22 August 2008; revised 4 December 2008; accepted 5 December 2008;
posted 10 December 2008 (Doc. ID 100474); published 9 January 2009

Wavelet analyses of tunable diode laser absorption spectroscopy signals were performed. The absorption spectroscopy data were obtained by repeatedly scanning the beams from a tunable diode laser operating in the near infrared across absorption lines of gaseous NH_3 contained within a windowed glass tube. The laser was modulated and wavelet analyses of the absorption data were performed. It was observed that harmonic wavelets could simultaneously extract the $1f$ and $2f$ harmonics as well as higher-order harmonics from the direct absorption data. © 2009 Optical Society of America

OCIS codes: 300.6260, 350.6980.

1. Introduction

Diode lasers have attracted widespread interest for detection of gaseous species because of their potential for rapid detection of low species concentrations with relatively low cost and robust laser systems [1,2]. Early applications used lasers that required operation at low temperatures, e.g., lead-salt lasers. More recently, near-IR telecommunications lasers that operate at room temperature have become popular because of their low cost.

Tunable diode laser spectroscopy is often performed by measurement of the direct absorption characteristics of atomic or molecular absorption lines. This is accomplished by scanning the laser frequency across individual absorption lines and measuring the laser attenuation as a function of frequency. In many cases, however, wavelength modulated spectroscopy (WMS) is used, e.g., in environments where noise levels are high or where absorption levels are small [3]. The WMS technique involves adding an oscillatory component to the laser as it is scanned across an absorption line. A lock-in amplifier is typically used to detect the oscillatory component or a harmonic, typically, the second harmonic ($2f$) signal is detected with a lock-in amplifier, though other harmonics can also be of interest. The WMS technique is generally considered to employ a modulation frequency that is less than the half-width frequency of the transition lineshape. Frequency modulation spectroscopy (FMS) uses a modulation frequency larger than the half-width frequency of the transition line shape [3].

This paper focuses on employing signal-processing techniques based on wavelet analyses of modulated signals obtained from tunable diode laser absorption spectroscopy (TDLAS) experiments. As will be shown, wavelets have the potential to enable detection of signal harmonics.

In Section 2, we will first present basic aspects of the theory related to Fourier analysis of absorption signals. In Section 3, fundamental aspects of wavelet analysis will be presented, followed by a description of the experiments (Section 4) and the analysis of the experimental results in Sections 5 and 6.

2. Fourier Analysis of TDLAS Signals

The Fourier analysis of TDLAS signals has been well described in the literature [3–8], so we will present only certain aspects here. To begin, consider an experiment where a laser beam with intensity $I_0(v)$ is directed across a sample of gas with the path length L. The laser frequency v is a function of the

0003-6935/09/020401-07$15.00/0

time t. The laser beam will be attenuated because of interactions with the gas, resulting in the beam intensity $I(\upsilon)$ at a detector. The beam intensities at any instant of time are assumed to be related through Beer's law (Eq. (1)):

$$I(\nu) = I_0(\nu)\exp(-\alpha L). \tag{1}$$

Here, α is the absorption coefficient, which depends on the laser frequency υ, i.e., $\alpha = \alpha(\upsilon)$. It is common to set $\alpha = \sigma C$, where σ is the absorption cross section and C is the concentration of absorbing molecules. If the absorption levels are small, i.e., I is only slightly smaller than I_0, then Eq. (1) can be linearized as shown in Eq. (2):

$$\alpha = -\frac{1}{L}\ln\left(\frac{I}{I_0}\right) = \frac{1}{L}\left(1 - \frac{I}{I_0}\right). \tag{2}$$

The absorption characteristics for an individual absorption line are generally assumed to be described by a Gaussian profile (applicable at low pressure), a Lorentzian profile (applicable at high pressures) or a Voigt profile (applicable at intermediate pressures). The Gaussian and Lorentzian profiles are described by relatively simple mathematical functions, but the Voigt profile is more complex, being a convolution of the Gaussian and Lorentzian profiles.

In these types of experiments, the laser frequency is slowly scanned across an absorption line while rapid frequency modulations are applied. If the laser is scanned slowly enough such that the mean laser frequency, denoted as $\bar{\nu}$, does not vary appreciably during one modulation period, then we can perform a Fourier analysis of the absorption signal under the assumption that the laser frequency during one period is described by Eq. (3):

$$\nu = \bar{\nu} + \varepsilon \times \cos(\omega t). \tag{3}$$

Here, the variable ε is the modulation amplitude and ω is the angular frequency of the modulation.

The Fourier analysis proceeds by expanding the absorption, α, in a Fourier cosine series:

$$\alpha = \sum_{n=0}^{\infty} H_n \cos(n\omega t), \tag{4}$$

where the coefficients H_n are evaluated as shown below:

$$H_0 = \frac{1}{2\pi}\int_0^{2\pi} \alpha \mathrm{d}\theta, \tag{5}$$

$$H_n = \frac{1}{\pi}\int_0^{2\pi} \alpha \times \cos(n\theta)\mathrm{d}\theta, \qquad n \geq 1. \tag{6}$$

In deriving Eqs. (5) and (6), we have introduced the angle $\theta = \omega t$ such that $\mathrm{d}\theta = \omega \mathrm{d}t$. The coefficients H_n can be evaluated experimentally by measuring the harmonics of the absorption signal with a lock-in amplifier at integer multiples of the modulation frequency. The case of $n = 2$ is generally of highest interest in WMS, though other harmonics are sometimes investigated. A focus of the present research is to demonstrate that wavelet analyses can be employed to gain information about the signal harmonics.

If the modulation amplitude, ε, is sufficiently small then α can be profitably expanded in a Taylor series:

$$\alpha[\bar{\nu} + \varepsilon \times \cos(\theta)] = \alpha(\bar{\nu}) + \varepsilon \times \cos(\theta)\left.\frac{\mathrm{d}\alpha}{\mathrm{d}\nu}\right|_{\nu=\bar{\nu}} + \frac{\varepsilon^2\cos^2(\theta)}{2}\left.\frac{\mathrm{d}^2\alpha}{\mathrm{d}\nu^2}\right|_{\nu=\bar{\nu}} + \ldots. \tag{7}$$

Substitution of Eq. (7) into Eq. (6) yields the following for $n = 2$:

$$\begin{aligned}\pi H_2 = {} & \alpha(\bar{\nu})\int_0^{2\pi}\cos(2\theta)\mathrm{d}\theta \\ & + \varepsilon\left.\frac{\mathrm{d}\alpha}{\mathrm{d}\nu}\right|_{\nu=\bar{\nu}}\int_0^{2\pi}\cos(\theta)\cos(2\theta)\mathrm{d}\theta \\ & + \frac{\varepsilon^2}{2}\frac{\mathrm{d}^2\alpha}{\mathrm{d}\nu^2}|_{\nu=\bar{\nu}}\int_0^{2\pi}\cos^2(\theta)\cos(2\theta)\mathrm{d}\theta \\ & + \frac{\varepsilon^3}{6}\left.\frac{\mathrm{d}^3\alpha}{\mathrm{d}\nu^3}\right|_{\nu=\bar{\nu}}\int_0^{2\pi}\cos^3(\theta)\cos(2\theta)\mathrm{d}\theta \\ & + \frac{\varepsilon^4}{24}\left.\frac{\mathrm{d}^4\alpha}{\mathrm{d}\nu^4}\right|_{\nu=\bar{\nu}}\int_0^{2\pi}\cos^4(\theta)\cos(2\theta)\mathrm{d}\theta + \ldots.\end{aligned} \tag{8}$$

Evaluation of the integrals in Eq. (8) yields the following:

$$H_2 = \frac{\varepsilon^2}{4}\left.\frac{\mathrm{d}^2\alpha}{\mathrm{d}\nu^2}\right|_{\nu=\bar{\nu}} + \frac{\varepsilon^4}{48}\left.\frac{\mathrm{d}^4\alpha}{\mathrm{d}\nu^4}\right|_{\nu=\bar{\nu}} + \frac{\varepsilon^6}{1536}\left.\frac{\mathrm{d}^6\alpha}{\mathrm{d}\nu^6}\right|_{\nu=\bar{\nu}} + \frac{\varepsilon^8}{92160}\left.\frac{\mathrm{d}^8\alpha}{\mathrm{d}\nu^8}\right|_{\nu=\bar{\nu}} + \ldots. \tag{9}$$

Similar expansions can be developed for other H_n coefficients. If ε is sufficiently small, the leading-order term in Eq. (9) will be dominant such that the second derivative of α with respect to ν will be linearly proportional to H_2 (see Eq. (10)). This limit is termed derivative spectroscopy:

$$H_2 = \frac{\varepsilon^2}{4}\frac{\mathrm{d}^2\alpha}{\mathrm{d}\nu^2}|_{\nu=\bar{\nu}}. \tag{10}$$

In situations that involve noisy environments, the signal-to-noise ratio can be increased by increasing ϵ.

The optimum value of ϵ depends on the harmonic that is being detected. For example, for Gaussian, Voigt, or Lorentzian absorption profiles, the absorption depth $m = \epsilon/\gamma$ should have a value of about 2.2 for optimal detection of the $2f$ signal [7–9], where γ is the half-width at half-maximum (HWHM) of the profile. This value of m is large enough that Eq. (10) is inapplicable. In general, for m of order unity or larger, the H_n integrals given by Eq. (6) must be evaluated directly. For example, analytical expressions for the H_n coefficients are available for Lorentzian [6,7] or Gaussian [8] absorption profiles. In general, the H_n coefficients are derivativelike in that they have the same general shape as $(\mathrm{d}^n\alpha/\mathrm{d}\nu^2)_{\nu=\bar{\nu}}$, i.e., they have the same number of zeros, maxima, and minima, but where these features appear at different values of $\bar{\nu}$.

3. Wavelet Analysis Techniques

Fourier analysis of a signal can provide information on the different frequencies that comprise the signal but not when these frequencies actually occur in time [10]. Techniques, such as windowed Fourier analysis, that involve analysis of only a portion of a signal can be used to provide information on the time dependence of frequency components, but these techniques suffer from a substantial lack of accuracy as the window width is decreased. Wavelet analyses have become popular in recent years as an alternative to Fourier analysis of signals. Wavelet analyses can provide more accurate information on how frequency components vary with time than techniques such as windowed Fourier analysis.

The continuous wavelet transform (CWT), denoted by W, of an absorption signal is defined as an integral [10] as shown in Eq. (11):

$$W(a,b) = \int_{-\infty}^{\infty} \alpha(t)\frac{1}{\sqrt{b}}\varphi\left(\frac{t-a}{b}\right)\mathrm{d}t. \tag{11}$$

Here, $\alpha(t)$ is absorption as a function of the time t (it is assumed that the laser frequency is known as a function of time), φ is a function that is termed the wavelet, a is a parameter that controls translation, and b is a parameter that controls scaling. As b increases the wavelet spreads out, enabling longer-scale features to be discerned. The function $\varphi(t)$ is called the mother wavelet and scaled and shifted versions of φ are termed daughter wavelets. Wavelets are generally localized such that, for fixed values of a and b, the integral in Eq. (11) is significantly influenced by $\alpha(t)$ in only a limited range of t. The wavelet transform transforms a one-dimensional signal, i.e., a signal that depends only on t, to a two-dimensional representation in terms of a and b. When W is small, the overlap between a and φ is small and, as the overlap between α and φ increases, then W also increases. In this sense, wavelet analysis can be considered to be a correlation technique, and the greater the value of W then the greater the correlation between α and φ. It is noted that wavelet transformations can also be considered to be band-pass filters, thus enabling frequency components of a signal to be determined within certain ranges. In practical cases it is often not possible to evaluate Eq. (11) with all possible daughter wavelets, and the discrete wavelet transform (DWT) is instead used where a subset of wavelets is employed by selecting discrete values of a and b.

The mother wavelet must satisfy the following conditions [11]:

$$\int_{-\infty}^{\infty} \varphi(t)\mathrm{d}t = 0, \tag{12}$$

$$\int_{-\infty}^{\infty} |\varphi(t)|^2\mathrm{d}t < \infty, \tag{13}$$

$$\int_{0}^{\infty} \frac{|\bar{\varphi}(f)|^2}{f}\mathrm{d}f < \infty. \tag{14}$$

In Eq. (14), $\bar{\varphi}(f)$ denotes the Fourier transform of $\varphi(t)$, as defined in Eq. (15):

$$\bar{\varphi}(f) = \int_{-\infty}^{\infty} \varphi(t)\exp(-2\pi i f t)\mathrm{d}t. \tag{15}$$

4. Experimental Methods

These experiments employed a tunable laser diode operating near 1527 nm, which corresponds to the near-infrared spectroscopic region. The laser diode is a fiber-pigtailed DFB Type 2 telecom laser with a nominal wavelength of 1527 nm and delivers 20 mW at room temperature and a driver current of 82 mA (Thorlabs, DFB1527.22-20). However, due to safety concerns, an attenuating (neutral density) filter was used to reduce the laser output power from 20 mW to 5 mW.

The laser diode was mounted on a 14-pin butterfly mount (Thorlabs, LM14S2) and driven by a compact benchtop thermoelectric temperature controller (Thorlabs, TED200). This particular temperature controller featured ripple and noise of less than 1 mA, with temperature resolution to 0.01 °C. This allowed the laser temperature to be controlled within 0.01 °C near 24 °C. Along with the temperature controller, the laser diode was driven by a benchtop laser current driver (Thorlabs, TD 200 V) with ripple noise of less than 1.5 μA, making laser line frequency fluctuations due to laser noise negligible. The current supply was scanned at 21.001 Hz with an average current of 50.2 mA (min = 41.9 mA, max = 58.7 mA) with a sawtooth ramp function. For wavelength modulation spectroscopy, a Stanford Research

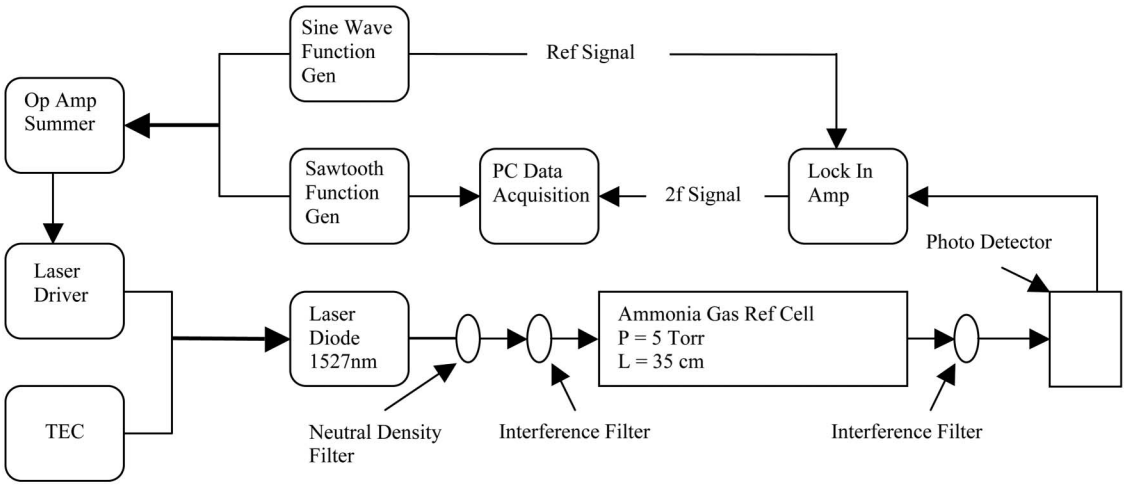

Fig. 1. Schematic of the WMS experimental setup.

510 lock-in amplifier was used to demodulate the absorption signal from a sealed ammonia gas reference cell. The reference cell had a nominal pressure of 5 torr and the cell length was 35 cm. In order to reduce the adverse affects of etalon interference fringes in the transmission path, 1 in. diameter 0.5° wedged fused silica windows were mounted at an angle of 3° at each end of the quartz cell. Because the gas reference cell was sealed, we were not able to vary the conditions within the cell to an appreciable extent. Figure 1 shows a schematic of the equipment used.

5. Basic Experimental Results

Figure 2 shows representative NH_3 absorption data obtained without modulation of the laser. The data in Fig. 2 show that there are two absorption lines present in the wavelength range investigated with the laser. These lines are consistent with NH_3 absorption lines reported in the literature [12,13]. Figure 3 shows representative data for the case where laser modulation was applied, and Fig. 4 shows $2f$ output from the lock-in amplifier.

6. Harmonic Wavelet Analysis of TDLAS Signals

For this analysis we have used harmonic wavelets as developed by Newland [14,15]. Harmonic wavelets, which have been used for a variety of signal analysis applications [14,15], can provide a time-frequency representation of a signal. In the time domain, harmonic wavelets are described by a complex function as follows:

$$\varphi(t) = \frac{\exp(4\pi it) - \exp(2\pi it)}{2\pi it}. \tag{16}$$

Here, $i = (-1)^{1/2}$. An interesting feature of harmonic wavelets is that, if they are Fourier transformed, the resulting function only allows frequencies within a discrete band to be passed. As a result, harmonic wavelets act as bandpass filters.

Harmonic wavelet analyses of TDLAS signals obtained in the present experiments were performed using procedures described in the literature [14,15], where it is noted that some steps involved the use of a fast Fourier transform (FFT). These analyses employed a DWT, such that specific bandpass frequency ranges resulted. The DWT analyses used $b = 2^{-j}$ and $a/b = k$, where j and k are integers related to scaling and translation. As j increases, the frequency resolution of the wavelet analysis increases. The lower and upper bandpass frequency limits for a given level j can be calculated using

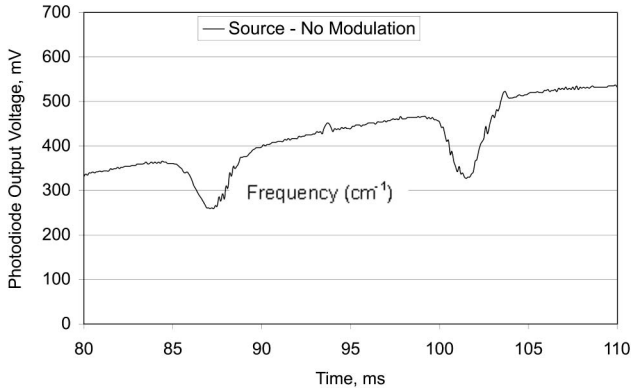

Fig. 2. Representative output from the photodiode without modulation of the laser.

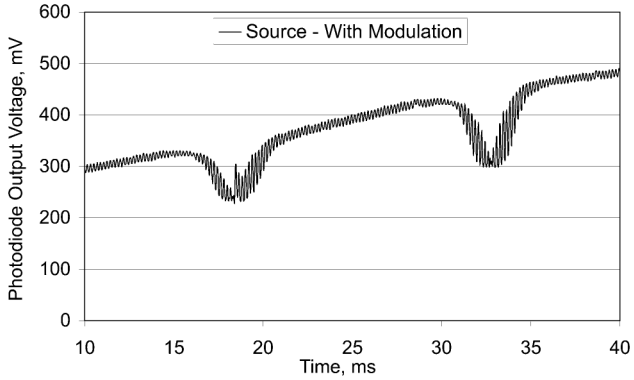

Fig. 3. Representative output from the photodiode with modulation of the laser.

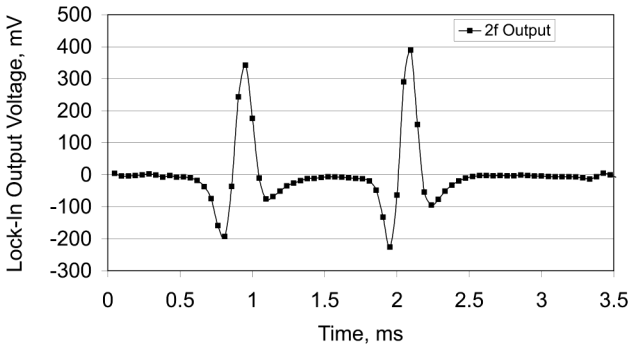

Fig. 4. Representative $2f$ output from the lock-in amplifier.

Eqs. (17) and (18):

$$f_{\min} = \frac{S}{N} 2^{j-1}, \tag{17}$$

$$f_{\max} = \frac{S}{N} 2^{j}. \tag{18}$$

Here, $f_{\min}$ is the lower bandpass frequency, $f_{\max}$ is the upper bandpass frequency, S is the digital sampling rate of the signal, and N is the number of data points in the signal. The bandwidth of a given level can be set to center about a particular signal frequency, e.g., the $2f$ frequency, by appropriate selection of S, N, and j. The index k is varied over certain ranges required for the harmonic wavelet analysis algorithms, as described in the literature [14,15].

Results from wavelet analyses of experimental results are shown in Figs. 5(a)–5(d) for the case where a data acquisition rate of $S = 100$ kHz was used and where the laser modulation frequency was $\omega/(2\pi) = 5$ kHz. The total number of data points was $N = 4096$ (not all data points are shown in Fig. 5 so that oscillations are more easily seen in the plots). Levels 8, 9, and 10 correspond to $j = 8$, 9, and 10, and the applicable wavelet bandpass frequency ranges are also noted in Fig. 5. Figure 5(a) shows the raw absorption data plotted as a function of time for one of the transitions. The next three plots [Figs. 5(b)–5(d)] show results from the wavelet analyses. The frequency range for Fig. 5(b) is such that the laser driving frequency (5 kHz) is passed, and the overall $1f$ signal shape corresponds approximately to the locus of points that correspond to the wave peaks, though, as noted later, the $1f$ signal can be discerned more clearly if the modulation (driving) signal is subtracted from the data in Fig. 5(b). The frequency range for Fig. 5(c) is such that the second harmonic signal (i.e., 10 kHz) is passed and the $2f$ signal shape can be clearly seen as the locus of points that correspond

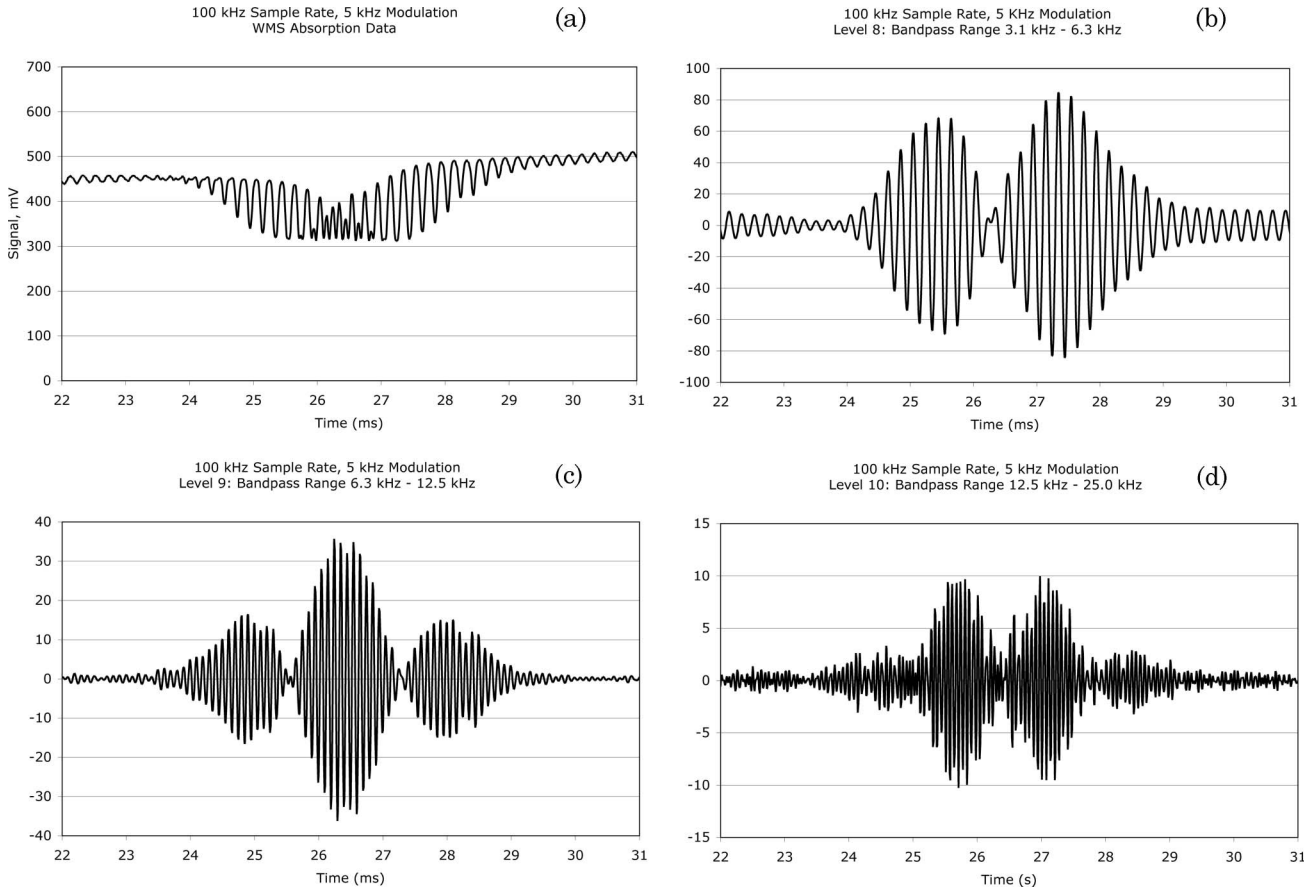

Fig. 5. Representative harmonic wavelet analysis results for different bandpass ranges.

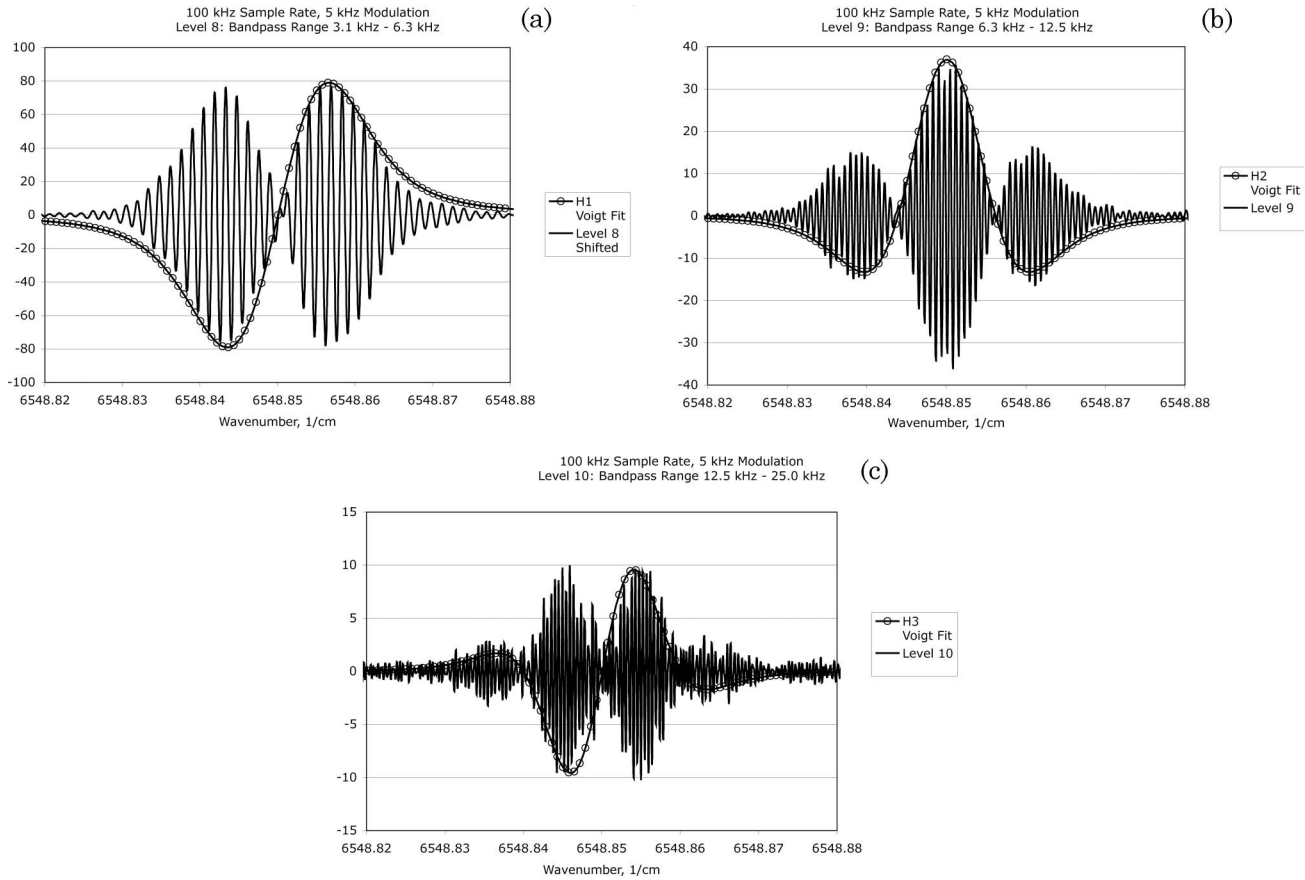

Fig. 6. Comparison of results from the wavelet analyses with (a) H_1, (b) H_2, and (c) H_3 coefficients obtained with a Voigt absorption profile.

to the wave peaks. The frequency range for Fig. 5(d) is large enough that the third and fourth harmonics (i.e., at 15 kHz and 20 kHz) are both present, but the signal will likely be dominated by the third harmonic such that the basic shape of the data will correspond most closely to the $3f$ signal. We assume that the third harmonic in Fig. 5(d) is dominant (relative to the fourth harmonic) because it is typically the case in Fourier analysis that the higher harmonics become more subdominant, which is consistent with the relative amplitudes of the data for each level in Figs. 5(b)–5(d) and also Fig. 6 (discussed below).

When using this type of wavelet analysis, it was observed that it is important to select the experimental parameters so that desired signal characteristics can be observed without interference. For example, if it is of interest to measure $2f$ signal characteristics, then N and S need to be selected such that the $2f$ signal is the only harmonic within a specific frequency range, as determined by Eqs. (17) and (18).

It is of interest to compare the wavelet analyses with analytical predictions for the overall shapes of the H_1, H_2, and H_3 signals. We have done this for the case of a Voigt absorption profile. Figures 6(a)–6(c) show plots of the level 8, 9, and 10 signals obtained with the harmonic wavelet analyses of the data, as well as plots of H_1, H_2, and H_3 for Voigt absorption profiles. Each level corresponds to a specific value of j, i.e., level 8 corresponds to $j = 8$. These profiles were generated by numerical integration of Eq. (6) via use of a commercial software package [16], and HWHM and absorption amplitudes were manually selected to provide good fits to the data in the time domain. In addition, the plots are presented in terms of wavenumbers instead of time.

It is apparent in these plots that the $1f$ and $2f$ signals obtained from the wavelet analyses correlate well with the basic functional forms of H_1 and H_2, indicating that the wavelet analyses performed well in terms of extracting the $1f$ and $2f$ harmonics. While still reasonable, the level 10 data do not show as good of agreement, which is likely a result of the fact that the level 10 data would have included both $3f$ and $4f$ data sets.

It is notable that the $2f$ data shown in Fig. 6(b) are symmetric about the center wavelength, unlike the $2f$ data obtained with the lock-in amplifier (Fig. 4). The asymmetry seen in Fig. 4 is a result of other harmonics (e.g., $1f$ and $3f$) appearing in the output of the lock-in amplifier with the $2f$ data. Evidently, the bandpass characteristics of the harmonic wavelet analyses performed here filter these harmonics out of the $2f$ data, resulting in a symmetric profile. It is of interest to investigate this behavior under other conditions, e.g., with different gases and under different partial pressures.

It is noted that, since the $1f$ data obtained with the wavelet analyses contain both the driving signal and the $1f$ signal, it is desirable to remove the driving signal from the $1f$ data. This was done in the present case by subtracting the driving signal directly from the wavelet data, where the driving signal was assumed to correspond to a sinusoidal function fit to the data in the far wings of the $1f$ wavelet signal. When this sinusoidal function was subtracted from the $1f$ wavelet data, the oscillations in the wings decayed quickly and the $1f$ signal became symmetric, as is evident in Fig. 6(a). This subtraction process was not applied to the $1f$ data in Fig. 5(b).

7. Conclusions

We have investigated the potential of using harmonic wavelets for analysis of signals from tunable diode laser spectroscopy experiments. Experimental data were obtained using a WMS system that was used to obtain absorption data on an isolated NH_3 spectral line near 1527 nm (6549 cm^{-1}). Analysis of the output from a photodiode showed that harmonic wavelets can be used to detect the $1f$, $2f$, and higher harmonics contained within the absorption signal.

It is of interest to extend this research by investigating other wavelets to determine whether there are other wavelet formulations that can provide usable information about TDLAS signals. Various gases at varied temperatures and pressures should also be investigated to determine the absorbance levels that can be detected with this technique, as well as to determine the utility of using wavelets in cases where significant broadening or overlap of spectral lines is present. Such research could potentially yield new methodology for spectroscopic analysis and detection of gases for analysis of time-dependent signal harmonics.

This research was supported in part by the University of California, Davis, and also by the National Aeronautics and Space Administration (NASA).

References

1. M. G. Allen, "Diode laser absorption sensors for gas-dynamic and combustion flows," Meas. Sci. Technol. **9**, 545–562 (1998).
2. K. Kohse-Höinghaus and J. B. Jeffries, *Applied Combustion Diagnostics* (Taylor and Francis, 2002).
3. O. Axner, P. Kluczynski, and A. M. Lindberg, "Theoretical description based on Fourier analysis of wavelength-modulation spectroscopy in terms of analytical and background signals," Appl. Opt. **38**, 5803–5815 (1999).
4. A. M. Russell and D. A. Torchia, "Harmonic analysis in systems using phase sensitive detectors," Rev. Sci. Instrum. **33**, 442–444 (1962).
5. G. V. H. Wilson, "Modulation broadening of NMR and ESR line shapes," J. Appl. Phys. **34**, 3276–3285 (1963).
6. R. Arndt, "Analytical line shapes for Lorentzian signals broadened by modulation," J. Appl. Phys. **36**, 2522–2524 (1965).
7. P. Kluczynski and O. Axner, "A general non-complex analytical expression for the nth Fourier component of a wavelength-modulated Lorentzian lineshape function," J. Quant. Spectrosc. Radiat. Transfer **68**, 299–317 (2001).
8. B. D. Shaw, "Analytical evaluation of the Fourier components of wavelength-modulated Gaussian functions," J. Quant. Spectrosc. Radiat. Transfer **109**, 2891–2894 (2008).
9. J. Reid and D. Labrie, "Second-harmonic detection with tunable-diode lasers—comparison with experiment and theory," Appl. Phys. B **26**, 203–210 (1981).
10. C. S. Burrus, R. A. Gopinath, and H. Guo, *Introduction to Wavelets and Wavelet Transforms—A Primer* (Prentice-Hall, 1997).
11. D. B. Percival and A. T. Walden, *Wavelet Methods for Time Series Analysis* (Cambridge U. Press, 2000).
12. L. Lundsberg-Nielsen, F. Hegelund, and F. M. Nicolaisen, "Analysis of the high-resolution spectrum of ammonia ($^{14}NH_3$) in the near-infrared region 6400–6900 cm^{-1}," J. Mol. Spectrosc. **162**, 230–245 (1993).
13. M. E. Webber, M. D. S. Baer, and R. K. Hanson, "Ammonia monitoring near 1.5 μm with diode-laser absorption sensors," Appl. Opt. **40**, 2031–2042 (2001).
14. D. E. Newland, "Harmonic wavelet analysis," Proc. R. Soc. London Ser. A **443**, 203–225 (1993).
15. D. E. Newland, "Harmonic wavelets in vibration and acoustics," Phil. Trans. R. Soc. London **357**, 2607–2625 (1999).
16. Mathematica 5.2, Wolfram Research, Inc., 100 Trade Center Drive, Champaign, Ill. 61820, USA.